Catal Lett (2009) 128:385–391
DOI 10.1007/s10562-008-9761-5

Fractal Extra-Framework Species in De-aluminated LaY Zeolites and Their Catalytic Activity

Pablo García · Enrique Lima · Julia Aguilar · Víctor Lara

Received: 17 September 2008 / Accepted: 30 October 2008 / Published online: 18 November 2008

Abstract Lanthanum-containing Y (LaY) zeolites were prepared by ionic exchange from NaY parent zeolite. The LaY zeolites were de-aluminated by steaming. De-aluminated zeolites presented different Si/Al ratio. The physicochemical properties of these catalysts were characterized by X-ray diffraction, pyridine and xenon adsorption, infrared spectroscopy and ^{29}Si, ^{27}Al, ^{129}Xe, ^{139}La solid-state nuclear magnetic resonance spectroscopy. Furthermore, a fractal geometry approach was adopted to describe the evolution in the texture as a consequence of de-alumination. The catalytic properties of materials were evaluated in the n-hexane cracking reaction. The catalyst with the highest catalytic activity was the zeolite highest de-aluminated (Si/Al ratio of 3.7). Such performance was attributed on the one hand, to active extra-framework aluminum species hosted in the large cavities of zeolites and, on the other hand to redistribution of lanthanum species into the zeolite as a consequence of de-alumination.

Keywords Porous · Zeolite · De-alumination · Xenon NMR · Acidity · Fractal

P. García · J. Aguilar
Universidad Autónoma Metropolitana, Azcapotzalco, Av. San Pablo 180, Col. Reynosa Tamaulipas, 02200 Mexico, DF, Mexico

E. Lima (✉) · V. Lara
Universidad Autónoma Metropolitana, Iztapalapa, Av. San Rafael Atlixco No. 186, 09340 Mexico, DF, Mexico
e-mail: lima@xanum.uam.mx

1 Introduction

Zeolites, a large family of microporous materials find applications in industrial and environmental fields, among others [1, 2]. Zeolites have been mainly used as molecular sieves, catalysts and catalyst supports. In this sense, they attracted major attention when such materials were used as highly active catalysts for various processes in the petroleum industry. Zeolites find many other industrial applications. For instance, Y type zeolites are used to catalyze reactions of cracking and alquilation [3, 4]. The faujasite zeolites (X and Y) framework consists of a three dimensional array of $(Si,Al)O_4$ tetrahedra. The basic unit of the structure is a polyhedron containing 24 tetrahedra which is called sodalite unit. These sodalite units are arranged in the same way as the carbon atoms in the lattice of diamond. The cubooctahedra are linked together by their hexagonal faces forming a hexagonal prism. These results in a series of wide, nearly spherical cavities called supercages or large cavities [5]. The catalytic performance of zeolites is mainly determined by their physicochemical properties and porosity [6, 7]. Physicochemical properties of zeolites can be modified by isomorphic substitutions of T atoms (Si, Al) into backbone aluminosilicate [8]. Such isomorphic substitutions are reached when zeolites are submitted to hard treatments such as fluorination and steaming, which are the main methods for de-alumination of zeolites [9]. The steaming consists in a thermal treatment of the zeolite in the presence of water steam; however this treatment can modify the Si/Al ratio. It is generally agreed that steaming promotes the removal of framework aluminum from zeolite structure to form amorphous aluminum oxides [10]. De-alumination induces modifications in the acidity as well as in the positions of the exchangeable cations into zeolite because of non-rigid character of such sites [11]. In order to characterize the

variation in acidity or cation positions, probe molecules and spectroscopy are highly suitable. Of course, these characterizations focus on a better knowledge of the catalytic sites. In the case of Y faujasite zeolite, xenon and pyridine are the most useful molecules probing the location of cations and acidity into the sites called large cavities, respectively [12, 13]. In this work we report the modification in structure, porosity, acidity and catalytic properties of lanthanum containing zeolites treated by steaming.

2 Experimental

2.1 Materials

Starting from a NaY zeolite, with a Si/Al ratio of 2.5, provided by GRACE DAVISON, two lanthanum containing zeolites (LaY) were prepared through cationic exchange in aqueous media. Then, de-aluminated zeolites were obtained by heating LaY zeolites under saturated water vapor. Typically, a de-alumination experiment was carried out as follows: 2 g of La-containing Y zeolite were placed in a tubular reactor where the sample was thermal treated under N_2 at 150 °C for 30 min. After that, the temperature was increased with a heating-rate of 5°/min until reached 800 °C; sample was maintained at this temperature and under a water vapor flow of 0.1 mL/s for 5 h. Two zeolites with different Si/Al ratio were obtained, Table 1. Samples were referred as LaY(X) where X indicates the La content (wt%).

2.2 Characterization

Catalysts were characterized by X-ray diffraction (XRD), small angle X-ray scattering (SAXS), Fourier transformed infrared spectroscopy (FTIR), pyridine and xenon adsorption, multinuclear (^{27}Al, ^{29}Si, ^{129}Xe, ^{139}La) solid-state nuclear magnetic resonance spectroscopy (NMR) and ^{129}Xe NMR in adsorbed phase.

XRD patterns were collected on a Siemens D-5,000 diffractometer using copper Kα radiation. From the XRD patterns the cell parameters of various catalysts were calculated (graphite was used as external reference).

SAXS experiments were performed using a Kratky camera coupled to a copper anode X-ray tube whose Kα radiation was selected with a nickel filter. The SAXS intensity data, I(h), were collected with a linear proportional counter. Then, they were processed with the ITP program [14–18] where the scattering vector is defined as $h = 4\pi\sin\theta/\lambda$, where θ and λ are the scattering angle and the X-ray wavelength, respectively. From the slope of the curve Log I(h) versus Log (h), the fractal dimension of the scattering objects was calculated [19].

For pyridine adsorption followed by FTIR, the catalyst samples were pressed in self-supporting thin wafers, and then activated at 200 °C, under vacuum; lastly the samples are contacted with an amount of pyridine vapor. Both 'clean sample' reference spectra and IR spectra after pyridine adsorption were collected at room temperature, as an average of 60 runs with 2 cm^{-1} resolution.

Solid-state ^{27}Al and ^{29}Si NMR single excitation spectra were performed at 78.3 and 59.59 MHz, respectively. ^{29}Si NMR spectra were acquired at 79.46 MHz on a Bruker Avance 400 spectrometer by using the combined techniques of magic angle spinning (MAS) and Proton Dipolar Decoupling (HPDEC). Direct pulsed NMR excitation was used throughout, employing 90° observing pulses (3 μs) with a pulse repetition time of 38 s. Powdered samples were packed in zirconia rotors. Spinning rate was 5 kHz. Chemical shifts were referenced to TMS.

^{27}Al MAS NMR spectra were acquired under MAS conditions using an ASX 300 Bruker spectrometer with a magnetic field strength of 7.05 T, corresponding to a ^{27}Al Larmor frequency of 78.3 MHz. Short single pulse ($\pi/12$) were used. The samples were spun at 10 kHz, and the chemical shifts were referenced to an aqueous 1 M $AlCl_3$ solution. The ^{139}La NMR spectra were obtained at 42.37 MHz using a t_1-τ-t_3 spin echo sequence with complex phase cycling [20, 21]. The associated $\pi/2$ pulse length was 10 μs. The acquisition parameters were: $t_1 = t_3 = 2.5$ μs. The chemical shifts were referenced to an external standard of saturated aqueous lanthanum

Table 1 Lanthanum content, cristallinity, cell parameter and the molar Si/Al ratio of different catalysts after steaming. The Si/Al ratio of starting zeolite was 2.5

Sample	% La (wt)	Cristalinity[a] (%)	Cell parameter[b] a (Å)	Si/Al molar ratio	
				^{29}Si MAS NMR	FTIR
LaY(3.0)	3.00	90	24.68	2.7	2.8
LaY(3.9)	3.90	85	24.50	3.7	4.0

[a] Graphite was the external reference

[b] As determined by XRD patterns

chloride. At least 200,000 scans were performed in order to have an acceptable signal/noise ratio.

Xenon gas (Praxair, 99.999%) was used for the ^{129}Xe NMR measurements. For these experiments, the sample powder was placed in a NMR tube equipped with valves, through which the xenon gas was equilibrated with the sample at 291 K under different pressures. Previously to xenon loading, samples were dehydrated by gradual heating up to 673 K in vacuum (1.33×10^{-4} kPa). ^{129}Xe NMR spectra were recorded at 291 K in a Bruker DMX-500 spectrometer operating at 138.34 MHz. Single excitation pulses were used and at least 1,000 scans were collected with a delay time of 2 s. The chemical shift was referenced to xenon gas extrapolated to zero pressure.

2.3 Catalytic Tests

The catalytic tests were performed in a microflow fixed-bed reactor using 50–100 mg of catalyst. Prior to any measurements, the catalysts were activated in situ under N_2 at 873 K during 12 h. n-hexane was fed through a saturator at 373 K. The reaction was carried out at 923 K and 1 atm. The reaction products were analyzed chromatographically using a Hewlett Packard 6,890 gas chromatograph.

3 Results and Discussion

Two zeolites containing different amount of lanthanum were prepared, Table 1. These samples, after the steaming treatment, turn to have different Si/Al molar ratio.

X-ray diffraction patterns, Fig. 1, did not show the formation of new crystalline phases upon de-alumination. The cell parameter was almost insensitive to de-alumination, only a very slight compression of zeolite unit cell was detected when Si/Al ratio varies from 2.7 to 3.7, Table 1; Of course a decreasing in the cristallinity was also detected because of the amount of dislodged silicon [22]. Migration of cations could occur [23] but detection of this feature is, in general, beyond of the detection limits of XRD technique. On the other hand, the NMR results support that short range modifications can be induced by the de-alumination. For instance, the Fig. 2 shows differences between the ^{29}Si MAS NMR spectra of two zeolites with different Si/Al ratio. It can be stated that zeolites are built by Si(4Al), Si(3Al), Si(2Al), Si(1Al) and Si(0Al) units, signals at −86, −92, −97, −102 and −108 ppm, respectively [24]. Si(nAl) units build the zeolite framework, where n is the number of aluminums bonded to tetrahedral silicon $(SiO_4)^{4-}$. Furthermore, from relative intensities ($I_{Si(nAl)}$) in the corresponding spectra and under the Lowenstein rule, which says that Al–O–Al bonds are forbidden, the Si/Al ratio (Table 1) was determined [25, 26], according to:

$$\frac{Si}{Al} = \frac{\sum_{n=0}^{4} I_{si(nAl)}}{\sum_{n=0}^{4} 0.25 n I_{si(nAl)}}$$

Note that, as a consequence of de-alumination it could be expected the creation of a high amount of defects with groups Si–OH and Al–OH. For instance, $Si(OAl)_n(OH)_{4-n}$ could be formed. In this context, resonances of this species are expected to be very close to those Si(nAl).

^{27}Al NMR spectra (Fig. 3) support further that typical tetrahedral aluminum (signal close to 50 ppm) of zeolite could leave the framework of zeolite. Thus extra-

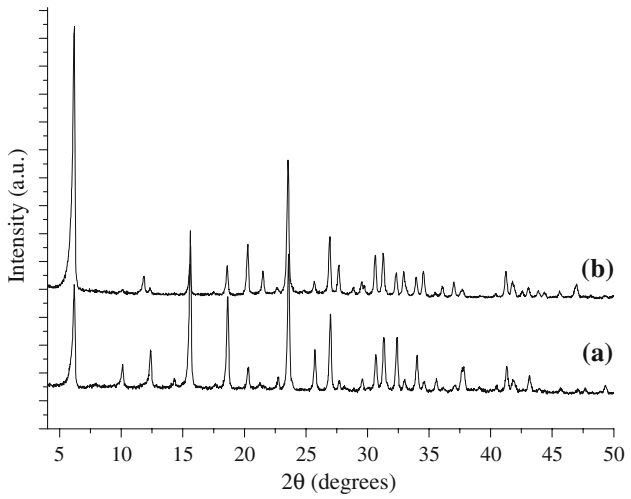

Fig. 1 X-ray powder diffraction patterns of sample LaY(3.9), before (**a**) and after (**b**) de-alumination treatment

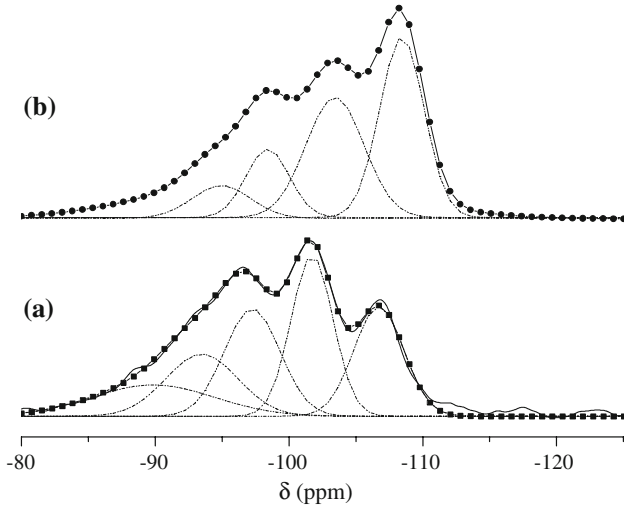

Fig. 2 ^{29}Si MAS NMR of LaY(3.0) and LaY(3.9) samples, **a** and **b**, respectively. The dotted lines correspond to each individual contribution and their sum is represented by the points. The solid line represents the experimental spectrum

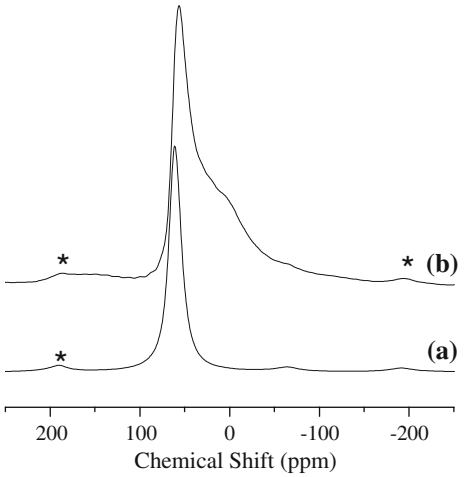

Fig. 3 ^{27}Al MAS NMR Spectrum of sample LaY(3.9), before (**a**) and after (**b**) de-alumination treatment. *Indicates spinning side bands

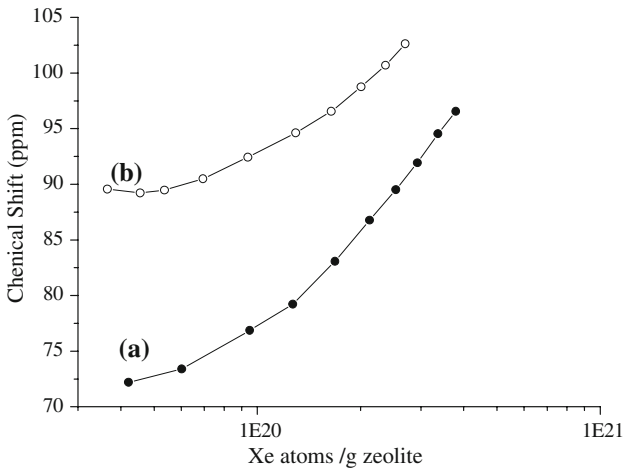

Fig. 5 Chemical shifts, δ, of ^{129}Xe NMR signals versus of xenon atoms adsorbed per gram of zeolite. Data for LaY(3.9) sample, before (–●–) and after (–◯–) de-alumination treatment

framework aluminum species, containing octahedral aluminum (broad signal between 30 and −10 ppm), appear. There is two possibilities to be located these extra-framework aluminum species: the first one is into the zeolite cavities [27] and the second one as a phase segregated at external surface.

In this context, ^{129}Xe NMR of xenon adsorbed in zeolites is the best probe molecule that permits to elucidate the presence of the extra-framework species in the large cavities of zeolite. Due to the sizes of the xenon atom and large cavities, xenon can only entry to the large cavity but not to sodalite cages of faujasite zeolites. The ^{129}Xe NMR spectra of xenon adsorbed in lanthanum-containing zeolites, before and after de-alumination, consisted of a single peak, Fig. 4. A significant difference should be noted: the peak before de-alumination is more asymmetric and broader than the

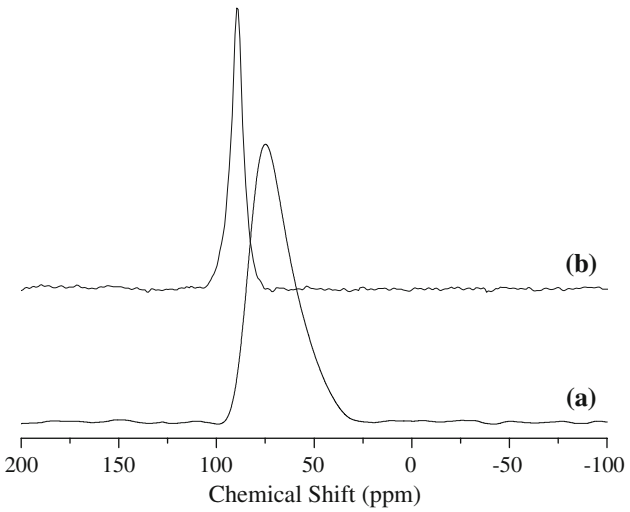

Fig. 4 ^{129}Xe NMR spectra of sample LaY(3.9), before (**a**) and after (**b**) de-alumination treatment. Samples were equilibrated under 0.2 atm of xenon gas. 5,000 scans were collected

corresponding one after de-alumination. It is worth mentioning that before de-alumination, different lanthanum-hydroxyl complexes can be stabilized inside the cavities. In Fig. 5 the chemical shift of the ^{129}Xe resonance is plotted as a function of the xenon loading. It is observed that de-aluminated zeolites exhibit higher chemical shifts than the non de-aluminated ones.

According to previous works [13, 28] the chemical shift of xenon in our samples can be expressed as follows:

$$\delta = \delta_0 + \delta_{\mathrm{Xe-W}} + \delta_{\mathrm{Xe-Xe}}$$

The observed chemical shift, δ, includes contributions of all interacting factors: δ_0 is the chemical shift of reference and has been fixed to zero, $\delta_{\mathrm{Xe-W}}$ is the parameter due to collisions between xenon atoms and zeolite walls, $\delta_{\mathrm{Xe-Xe}}$ is caused by xenon–xenon collisions. This last term determines the value of δ at high loading of xenon; in contrast, at low xenon loading the interactions between xenon and pore-wall are the main contributions to the chemical shift. $\delta_{\mathrm{Xe-W}}$ value is expected to be different for aluminated and de-aluminated because of the different nature of walls in both zeolites.

From Fig. 5, the $\delta_{\mathrm{Xe-W}}$ increases with de-alumination, suggesting thus that xenon atoms in cavities of the de-aluminated zeolites senses a higher electron density that the non de-aluminated one. In other words, the xenon atoms in supercages of the de-aluminated LaY zeolite is submitted to stronger interactions with wall of zeolite due to decreasing of volume of the supercage and, consequently, to the presence of extra-framework species. From these results a conclusion emerges: extra-framework aluminum species are stabilized in the large cavities of the zeolites. This feature implies that the size of large cavity is modified. The value of $\delta_{\mathrm{Xe-W}}$ has been correlated as an

Table 2 Average pore diameter obtained from ^{129}Xe NMR data

Sample	Before steaming		After steaming	
	$\delta_{n\to 0}$ (ppm)	Pore diameter (Å)	$\delta_{n\to 0}$ (ppm)	Pore diameter (Å)
LaY(3.0)	69	14.9	81	12.1
LaY(3.9)	73	13.8	91	10.3

inverse function of the mean free path ($\langle L \rangle$) for a Xe atom within the pore. Such dependence has been pointed out through the following empirical expression [29]:

$$\delta_{n\to 0} = (243)(0.2054)/(0.2054 + \langle L \rangle)$$

In the case of lanthanum-containing zeolites, the de-alumination caused a variation in the mean free path of the xenon, Table 2. Indeed, since the large cavities of faujasite zeolites can be view as spheres, this estimated $\langle L \rangle$ value corresponds to a pore diameter of 14.9 Å for the LaY(3.0) sample (before de-alumination) but this value decrease almost 3 Å after de-alumination. Data included in Table 2 are easily interpreted: as a consequence of the hosting of the extra-framework aluminum species there is a reduction in the micropore size. Mean pore diameter in Table 2 is the effective pore size that the Xe atom senses.

Up to this point results seem to show extraction of aluminum from backbone of zeolites and the apparition of extra-framework species stabilized into the free spaces. Nevertheless, the extraction of aluminum implies that connectivity of the lattice is modified. In this sense, many phenomena in the real world are best modeled by geometric structures that are much more irregular than Euclidean geometry [30]. One of the most common example is the Sierpinski gasket which is the connected subset of the plane obtained from an equilateral triangle by removing the open middle inscribed equilateral triangle of 1/4 the area, removing the corresponding open triangle from each of the three constituent triangles, and continuing this way [31]. In our case, zeolites are objects which are surfaces that, of course, exist in a three dimensional world. Fractal dimension is a valuable parameter to understand the degree of imperfections in the zeolite lattice [32]. Note that, the presence of extra-framework species in cavities reduces the connectivity of the lattice, i.e. the "perfect" walls of cavities become "imperfect". Thus fractal dimension of various samples were determined from SAXS data, Fig. 6 and Table 3. Upon de-alumination, the fractal dimension increases revealing that extra-framework species reduce the connectivity of the lattice obstructing cavities, in agreement with interpretation of ^{129}Xe NMR data. Indeed, if the chemical shift due to collisions between xenon atoms and pore-wall (δ_{Xe-W}) is plotted as a function of fractal dimension, a linear trend is obtained (Fig. 7).

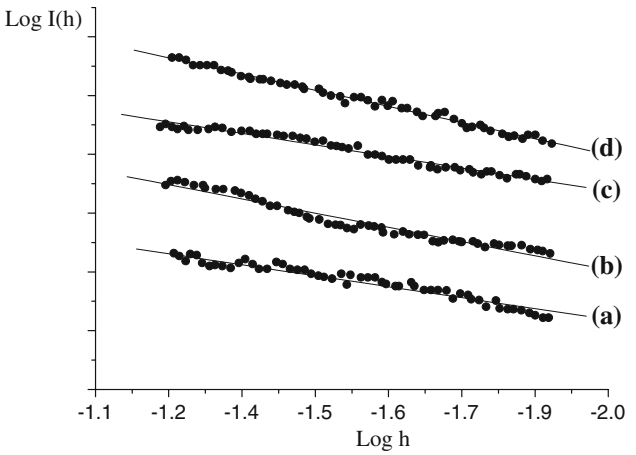

Fig. 6 SAXS curves to obtain the fractal dimension of LaY(3.0), before (**a**) and after (**b**) de-alumination and of LaY(3.9), before (**c**) and after (**d**) de-alumination

Table 3 Fractal dimension as determined by SAXS data

Sample	Fractal dimension	
	Before steaming	After steaming
LaY(3.0)	1.91	2.34
LaY(3.9)	2.03	2.71

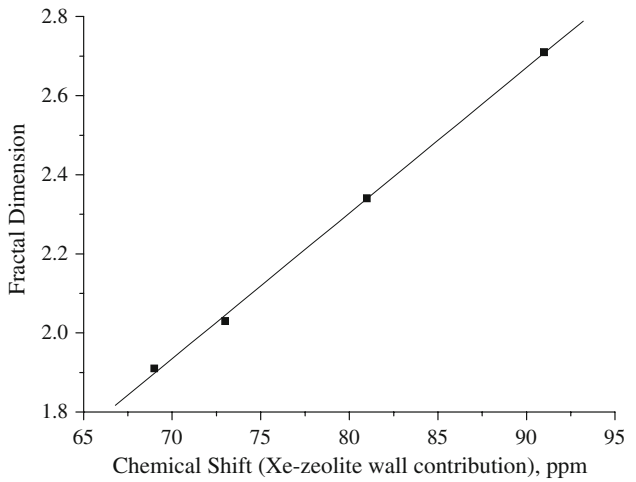

Fig. 7 Dependence of δ_{Xe-W} with fractal dimension (δ_{Xe-W} is the contribution to ^{129}Xe NMR signal due to collisions between xenon atoms and zeolite walls)

Such dependence reveal that degree of imperfection of surface is a consequence of the extraframework species located into the large cavities. On the one hand xenon is sensitive to changes into the zeolitic cavities and on the other the fractal dimension is also determined by the level of destruction of zeolitic cavities as a consequence of de-alumination process.

We return now, to the asymmetric ^{129}Xe NMR signal observed before de-alumination which suggests that signal is composed by two peaks. This results support that lanthanum cations are not homogeneously distributed into the free spaces. Moreover, after de-alumination a single peak is observed revealing that extra-framework species and cations turn to be homogeneously distributed inside the large cavities.

Thus, NMR of xenon adsorbed shows that, as a consequence of the formation of extra-framework species, a migration of cations into the zeolite can occur, which could be expected because of the non-rigid positions of the compensating cations [23]. In this sense, the lanthanum cations in both catalysts should be redistributed in the various zeolitic cages. ^{139}La NMR spectra suggest such migration. Figure 8 shows the spectrum of sample, before de-alumination, composed by a single peak centered close to −36 ppm, which was previously assigned to lanthanum cations in the supercages [21]. With de-alumination, the spectrum is significantly modified; the signal close to −36 ppm decreases its intensity and appears superimposed in a very broad line. This variation is explained as a migration of the lanthanum cations as a consequence of de-alumination. Indeed, the very broad line appears because lanthanum, a quadrupolar nucleus, should be located in different environments, i.e. in different sites of the zeolite framework, including supercages and sodalite cages. Of course MQ MAS spectra would confirm if the broadening of La NMR signal is or is not quadrupolar in nature. Such experiments are suitable to be carried out at high magnetic fields and unfortunately this is the reason which we are unable to make them. However, previously Herreros et al. [21] have explained this broadening of line as migration of cations as explained above, such migration is possible because before de-alumination lanthanum cations are hydrated and its average size is close to 4 Å. The sodalite cages are inaccessible (pore entrances of 2.4 Å). However during steaming treatment the vibrations of zeolite lattice increases and at same time the hydration sphere of cations can be lost; these two features could make possible the migration of cations from supercages to sodalite cavities.

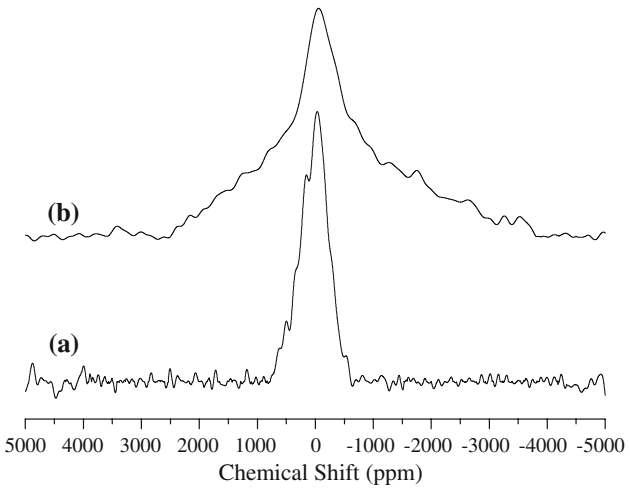

Fig. 8 Static ^{139}La NMR spectra of sample LaY(3.9), before (**a**) and after (**b**) de-alumination treatment

In summary, NMR results support that extra-framework enriched-aluminum species are formed in the large cavities of zeolite and then a redistribution of lanthanum cations occurs upon de-alumination. The participation of these extra-framework species in the catalysis of the hexane cracking remains opened.

Catalytic activity of de-aluminated LaY(3.0) and LaY(3.9) catalysts in the hexane cracking is reported in Table 4. Two remarks should be noted, the first one is the higher the Si/Al ratio the higher is the activity. The second one is that selectivity to heavier hydrocarbons (C5) is favored with the catalyst most active. Nevertheless a great amount of (C4) was detected in this catalyst. In order to disclose on the activity of this catalyst, the mixture C4 was characterized, then a great amount (70%) of butane was detected; most probably the reaction isomerization reaction i-butane towards butane is favored because of the availability of the acid sites, claimed for this reaction. Thus acidity in these two catalysts is different as suggested by the characterization and catalysis results. Of course the Turnover number, defined as the catalytic activity per aluminum into lattice, increases with de-alumination. This suggests that the amount of strong acid sites increases with de-alumination. The amount of aluminum sites playing the role of acid sites increases with de-alumination. In this context, the strength of these sites also varied as pointed out by the adsorption–desorption of pyridine followed by infrared spectroscopy, Fig. 9. In such a figure the relation between intensities of bands due to pyridine adsorbed in Bronsted and Lewis acid sites is plotted as a function of the desorption pyridine temperature. Note that catalyst LaY(3.9) always exhibits a higher ratio $I_{Bronsted}/I_{Lewis}$ even at temperatures as high as 400 °C, suggesting that stronger acid sites are present on this catalyst than the others one. Actually, a molecular dynamic simulation [33] has reported different extra-framework species that could be present as

Table 4 Activity and selectivity exhibited by catalysts in hexane cracking reaction

Catalyst	Activity 10^{-3} mol g^{-1} h^{-1}	**Selectivity (%)			
		C1 + C2	C3	C4	C5
LaY(3.0)	8	25.2	10.3	11.6	52.9
LaY(3.9)	66	4.1	34.7	64.5	2.2

* Ci = hydrocarbons; where i = number of carbons

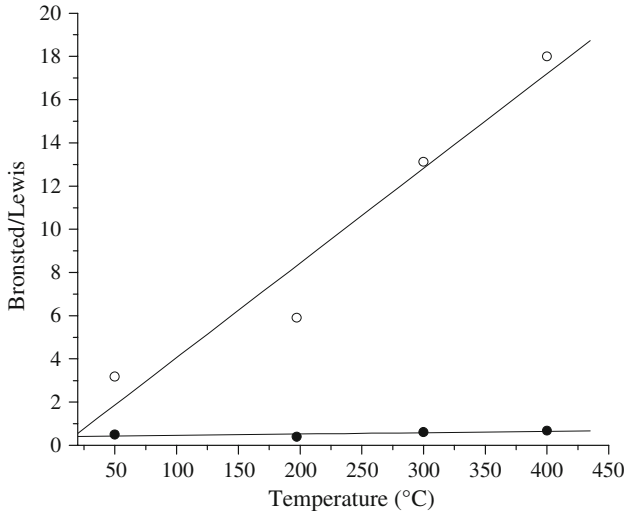

Fig. 9 Relation of intensities of infrared absorption bands assigned to pyridine adsorbed in Bronsted and Lewis acid sites. (–●–)Sample LaY(3.0) and (–◯–) Sample LaY(3.9)

zeolites are de-aluminated. The mechanism of formation of this extra-framework Al_2O_3 species includes the breaking of Al–O bonds and appearance of dangling oxygens bonded to the neighboring silicon atoms. At this time, the steaming could leads to formation of acid OH groups. These hydroxyls could lead to formation of Si–OH or Al–OH groups. ^{1}H–^{29}Si CP MAS NMR spectra (not shown) did not reveal an increasing of silanol groups as a consequence of de-alumination, then Al–OH groups could be mainly created. Furthermore, it is worth mentioning that ^{139}La NMR suggested that de-alumination induces changes on the position of lantahanum cations, thus it could be reasonably assumed that de-alumination influences the amount of acid sites but also their redistribution into the zeolite.

4 Conclusion

De-alumination of lanthanum-containing zeolites throughout steaming leads to an increasing in Si/Al framework ratio. With steaming, a reduction in the pore is detected by the xenon molecular probe. Furthermore, as a consequence of de-alumination the lanthanum cations are redistributed in the exchangeable positions of zeolites. The extracted aluminum can be hosted in the larges cavities of zeolites and then act as acid sites, which, indeed, are available to catalyze chemical reactions.

Acknowledgment Thanks are due to Conacyt for grant 24676.

References

1. Fu CM, Korchak VN, Hall WK (1981) J Catal 68:166
2. Chiche B, Finiels A, Gauthier C, Geneste P, Graille J, Pioch D (1986) J Org Chem 51:2128
3. Sivasanker S, Thangaraj A (1992) J Catal 138:386
4. Suzuki M, Tsutsumi K, Takahashi H, Saito Y (1988) Zeolites 8:284
5. Breck DW (1974) Zeolite molecular sieves. J Wiley Sons, New York
6. Kärger J, Ruthven D (1992) Difussion in zeolites and other microporous solids. J Wiley Sons, New York
7. Rouquerol F, Rouquerol J, Sing K (1999) Adsorption by powders and porous solids. Academic Press, London U.K
8. Zicovich-Wilson C, Corma A (2000) J Phys Chem B 104:4134
9. Fan Y, Lin X, Shi G, Liu H, Bao X (2007) Micr Mes Mater 98:174
10. Kerr G (1967) J Phys Chem B 72:4155
11. Lima EJ, Ibarra IA, Vera MA, Lara VH, Bosch P, Bulbulian S (2004) J Phys Chem B 108:12103
12. Maache M, Janin A, Lavalley JC, Joly JF, Benazzi E (1993) Zeolites 13:419
13. Ito T, Fraissard J (1982) J Chem Phys 76:5225
14. Glatter O (1991) Prog Colloid Polym Sci 84:46
15. Glatter O (1988) J Appl Cryst 21:886
16. Glatter O (1981) J Appl Cryst 14:101
17. Glatter O, Gruber K (1993) J Appl Cryst 26:512
18. Glatter O, Hainisch B (1984) J Appl Cryst 17:435
19. Harrison A (1995) Fractals in Chemistry. Oxford University Press Inc, New York
20. Kunwar A, Turner G, Oldfield E (1986) J Magn Reson 69:124
21. Herreros B, Man PP, Manoli J-M, Fraissard J (1992) J Chem Soc Chem Commun 464
22. Siantar D, Millman W, Fripiat J (2000) Zeolites 15:556
23. Shy D, Chen S, Lievens J, Liu S, Chao K (1991) J Chem Soc Faraday Trans 87:5855
24. Lippmaa E, Magi M, Samoson A, Engelhardt G, Grimmer AR (1980) J Am Chem Soc 102:4889
25. Loewenstein W (1954) Am Mineral 39:92
26. Fyfe CA, Gobbi GC, Murphy WJ, Ozubko RS, Slack DA (1984) J Am Chem Soc 106:4435
27. Coster D, Fripiat JJ (1993) Chem Mater 5:1204
28. Fraissard J, Ito T (1988) Zeolites 8:350
29. Demarquay J, Fraissard J (1987) Chem Phys Lett 136:314
30. Szeliskit R, Terzopoulos D (1989) Comput Graph 23:51
31. Kigami J (1989) Appl Math 8:259
32. Lima EJ, Lara VH, Bulbulian S, Bosch P (2004) Chem Mater 16:2255
33. Álvarez LJ, Ramírez-Solís A, Bosch P (1997) Zeolites 18:54